HHS Public Access

Author manuscript

Eur Psychiatry. Author manuscript; available in PMC 2017 April 24.

Published in final edited form as:

Eur Psychiatry. 2016 August ; 36: 55–64. doi:10.1016/j.eurpsy.2016.03.003.

Comparison of electric field strength and spatial distribution of electroconvulsive therapy and magnetic seizure therapy in a realistic human head model

Won Hee Lee[1], **Sarah H. Lisanby**[2,3,4,5], **Andrew F. Laine**[6], and **Angel V. Peterchev**[2,7,8,*]

[1]Department of Psychiatry, Icahn School of Medicine at Mount Sinai, New York, NY 10029, USA

[2]Department of Psychiatry and Behavioral Sciences, Duke University, Durham, NC 27710, USA

[3]Department of Psychology & Neuroscience, Duke University, Durham, NC 27708, USA

[4]Department of Psychiatry, Columbia University, New York, NY 10032, USA

[5]National Institute of Mental Health, National Institutes of Health, Bethesda, MD 20892, USA

[6]Department of Biomedical Engineering, Columbia University, New York, NY 10027, USA

[7]Department of Biomedical Engineering, Duke University, Durham, NC 27708, USA

[8]Department of Electrical and Computer Engineering, Duke University, Durham, NC 27708, USA

Abstract

Background—This study examines the strength and spatial distribution of the electric field induced in the brain by electroconvulsive therapy (ECT) and magnetic seizure therapy (MST).

Methods—The electric field induced by standard (bilateral, right unilateral, and bifrontal) and experimental (focal electrically administered seizure therapy and frontomedial) ECT electrode configurations as well as a circular MST coil configuration was simulated in an anatomically realistic finite element model of the human head. Maps of the electric field strength relative to an estimated neural activation threshold were used to evaluate the stimulation strength and focality in specific brain regions of interest for these ECT and MST paradigms and various stimulus current amplitudes.

Results—The standard ECT configurations and current amplitude of 800–900 mA produced the strongest overall stimulation with median of 1.8–2.9 times neural activation threshold and more than 94% of the brain volume stimulated at suprathreshold level. All standard ECT electrode

*Correspoinding Author: Department of Phychiatry and Behavioral Sciences, Duke University, Box 3620 DUMC, Durham, NC 27710, USA, angel.peterchev@duke.edu, Tel: +1 919 684 0383, Fax: +1 919 681 9962.

Financial Disclosures

W. H. Lee reports no relevant financial disclosures. S. H. Lisanby has served as Principal Investigator or co-investigator on industry-sponsored research grants to Duke (Brainsway, NeoSync, Nexstim); equipment loans to Duke (Magstim, MagVenture); is co-inventor on a patent and patent applications on TMS/MST technology; has been supported by grants from NIH (R01MH091083, U01MH084241, R01MH060884), Stanley Medical Research Institute, US Air Force, and Brain and Behavior Foundation; and has no consultancies, speakers bureau memberships, board affiliations, or equity holdings in related industries. A. F. Laine reports no relevant financial disclosures. A. V. Peterchev is inventor on patents and patent applications on TMS technology; has received research and travel support as well as patent royalties from Rogue Research for TMS technology, research and travel support from Tal Medical related to TMS technology, patent application support from Magstim, as well as TMS and MST equipment loans from MagVenture.

placements exposed the hippocampi to suprathreshold electric field, although there were differences across modalities with bilateral and right unilateral producing respectively the strongest and weakest hippocampal stimulation. MST stimulation is up to 9 times weaker compared to conventional ECT, resulting in direct activation of only 21% of the brain. Reducing the stimulus current amplitude can make ECT as focal as MST.

Conclusions—The relative differences in electric field strength may be a contributing factor for the cognitive sparing observed with right unilateral compared to bilateral ECT, and MST compared to right unilateral ECT. These simulations could help understand the mechanisms of seizure therapies and develop interventions with superior risk/benefit ratio.

Keywords

Unipolar depression; Mania and bipolar disorder; MRI; ECT; Transcranial magnetic stimulation (TMS)

1. Introduction

Electroconvulsive therapy (ECT) is a highly effective treatment that induces a generalized seizure in anesthetized patients by administering electric current to the brain via scalp electrodes. ECT has unparalleled antidepressant efficacy in the treatment of severe major depression [1]. However, its clinical use is limited by cognitive side effects such as retrograde amnesia [2–4]. Advances in ECT technique have reduced the side effects of ECT. These include the shift from long sinewave pulses to brief rectangular pulses [5, 6] and subsequently to ultrabrief pulses [7–10] which reduced the strength of neural stimulation in the brain and improved tolerability (see review in [4]). As well, changes in electrode placement can reduce cognitive side effects. High-dose right unilateral (RUL) ECT has a comparable efficacy to bilateral (BL) ECT with a significant decrease in amnesia [11], potentially due to the increased focality of the RUL stimulus [12]. Other electrode configurations that increase focality and target frontal brain regions include bifrontal (BF) ECT [13] and experimental paradigms such as focal electrically administered seizure therapy (FEAST) [14, 15] and frontomedial (FM) ECT [16]. However, even with relatively focal electrode placements, conventional ECT current amplitudes of 800–900 mA generate an electric field (E-field) strength that is substantially above the threshold for neural firing of most of the brain, and hence produce stimulation that is both non-focal and more intense than necessary for seizure induction [17]. Reducing the stimulus current amplitude can therefore make the ECT E-field more focal and closer to the neural firing threshold [12, 18], while still being able to elicit generalized seizures, although the efficacy and side effects of such paradigms have been explored to a very limited extent in early studies [19] as well as recent small studies and case reports [14, 16, 20–22]. Such E-field characteristics are also achieved in magnetic seizure therapy (MST) which uses high-dose repetitive transcranial magnetic stimulation to induce a seizure, is associated with fewer cognitive side effects than conventional ECT, and has shown therapeutic efficacy in several studies [23–27]. For these conventional and experimental interventions, there is insufficient knowledge of the characteristics of the E-field induced in the brain by the various electrode and coil

configurations as well as current amplitudes, which limits our ability to understand the mechanisms of these interventions and to rationally optimize their dosing.

Previously, using a spherical head model, we examined the stimulation strength and directly stimulated subvolume of the brain (focality) of various ECT electrode and MST coil configurations [17], showing that the E-field strength relative to threshold for MST is 3–6 times weaker and 10–60 times more focal compared with conventional ECT with 800 mA, 0.3 ms pulses. Spherical head models, however, are limited by the substantial simplification of the head anatomy, tissue heterogeneity, and anisotropic tissue properties. In another study using a realistic human head model, we investigated the induced E-field strength in various brain regions of interest (ROIs) by the BL, BF, RUL, and FEAST ECT electrode configurations [28]. However, that study used a truncated head model above the level of the auditory canal, and FM ECT and MST were not modeled. To date, the E-field generated by MST has not been studied in a realistic head model. Moreover, our prior study [28] and other ECT simulations in realistic head models [29, 30] did not explore the E-field characteristics relative to neural activation threshold or the effect of current amplitude adjustment.

Addressing these questions, in this paper we extend our previous work to investigate the characteristics of the E-field induced in the brain by ECT and MST. We create an anatomically realistic finite element model of the whole head to simulate the E-field distribution induced by various ECT electrode configurations and an MST coil configuration. We evaluate and compare the stimulation strength and focality relative to an estimated neural activation threshold in the whole brain as well as in specific ROIs thought to be associated with therapeutic action and/or adverse side effects of ECT and MST. Finally, we consider the effect of the stimulus current amplitude on stimulation strength and focality. These simulations could help the interpretation of clinical studies and may guide the improvement of ECT and MST dosing paradigms.

Preliminary results from this study were previously presented in part in conference proceedings [31].

2. Materials and methods

2.1. Data acquisition and image preprocessing

The head model was derived from magnetic resonance imaging (MRI) data of one healthy human subject (male, right handed, age = 34 years). Written informed consent approved by the Institutional Review Board of Columbia University was obtained from the subject before the experiments. T1-weighted structural MRI and diffusion tensor imaging (DTI) datasets of this subject, including the skull base and a portion of the neck underneath, were acquired on a 3 T Philips Achieva scanner (Philips Medical Systems, Best, Netherlands) using an 8-channel head coil. A three-plane localizer and sagittal scout image were acquired to determine the location of the anterior commissure (AC) and posterior commissure (PC). The T1-weighted MRI images were obtained with a 3D spoiled gradient recalled echo (SPGR) (TR = 6.5 ms; TE = 3.0 ms; 256 coronal slices; 1×1×1 mm^3 voxel; FA = 8°; 2 averages). We corrected the structural MRI image intensities for bias field inhomogeneity [32]. We then

applied content-preserving anisotropic diffusion filtering to remove the image noise or artifacts while preserving content details and improving tissue boundaries [33, 34].

The DTI data were acquired by employing a single-shot spin-echo echo-planar imaging (EPI) sequence (TR = 13510 ms; TE = 70 ms; 112×112 acquisition matrix; FA = 90°; 2×2×2 mm^3 voxel). The diffusion sensitizing gradients with a b-value of 1000 s/mm^2 were applied in 32 non-collinear directions. We corrected the DTI data for distortions due to eddy currents and subject motion artifacts. The diffusion tensor volumes were then co-registered to the T1-weighted MRI volume while the orientation of each diffusion tensor was preserved using the FSL's diffusion toolbox (FDT) from the FMRIB Software Library (FMRIB Analysis Group, University of Oxford, UK).

2.2. Tissue segmentation

To create a realistic volume conductor model of the whole head, the structural MRI images were segmented into several tissue regions (see Table 1). We first removed non-brain regions using the skull-stripping algorithm of the BET tool in FSL [35]. This initial segmentation was further corrected for accurate brain extraction using manual editing tools in the ITK-SNAP software [36]. The de-skulled MRI images were automatically segmented into subvolumes corresponding to gray matter, white matter, and cerebrospinal fluid (CSF) using the automated segmentation tool FAST in FSL [37]. The non-brain regions were manually segmented into 11 different tissue regions, including skin, muscle, skull compacta, skull spongiosa, vertebrae, spinal cord, lens, eyeball, sclera, optic nerve, and sinus, using a combination of segmentation editing tools of ITK-SNAP [36] and an in-house segmentation algorithm based on thresholding and mathematical morphological operations [28, 33, 34]. The complete head model and its constituent tissues are displayed in Figure 1.

2.3. ECT electrode and MST coil configurations

For ECT, three conventional ECT electrode configurations (BL, BF, and RUL) [13] and two experimental configurations (FEAST and FM) [14, 16] were modeled (see Figure 2). For BL ECT, the two electrodes were placed bilaterally at the frontotemporal positions located 2.5 cm above the midpoint of the line connecting the external canthus and tragus. For BF ECT, the electrodes were positioned bilaterally 5 cm above the outer angle of the orbit on a line parallel to the sagittal plane. For RUL ECT, one electrode was placed 2.5 cm to the right of vertex and the second electrode were placed in the right frontotemporal position. For FEAST, a wide rectangular electrode (2.5 cm × 6.3 cm) was placed over the right motor strip and a small circular electrode (2 cm diameter) was placed over the right eyebrow [14]. For FM ECT, one electrode was placed medially on the forehead and the second electrode was placed in front of vertex [16].

For MST, we modeled a circular coil placed on vertex (CIRC, S/N MP39, Magstim Co, Whiteland, Wales, UK) using manufacturer's data and inductance measurements [17, 38]. The CIRC coil consists of two parallel layers of windings connected electrically in series, each with an inner diameter of 44 mm, outer diameter of 120 mm, and 9 turns (see Figure 2). The coil conductors were centered above the vertex of the head model. Even though frontal

placement of this coil has been studied as well, vertex stimulation appeared to be more effective in inducing seizure activity [38].

2.4. Tissue electrical conductivity

All tissue regions were considered electrically isotropic except the white matter. The electrical conductivity values for the isotropic tissue compartments are given in Table I [28, 34, 39–42]. These values correspond to the relatively low frequencies (1–3 kHz) that dominate both the ECT and MST pulse spectra. To estimate the white matter conductivity tensors σ with variable anisotropy ratios, we deployed the volume normalized technique using the measured diffusion tensors D and the isotropic white matter conductivity σ_{iso} [43–46]. The diffusion tensor in each voxel is linearly scaled so that the volume of the conductivity tensor equals that of an isotropic conductivity sphere with radius σ_{iso}

$$\sigma = \frac{\sigma_{iso}}{\sqrt[3]{d_1 \cdot d_2 \cdot d_3}} D \quad (1)$$

where d_i are the diffusion tensor eigenvalues. This approach preserves variable anisotropy ratios (eigenvalue ratios) over the white matter regions and the orientation (eigenvectors) of diffusion tensors.

2.5. Electric field computation

To obtain the E-field distribution induced in the brain by the various ECT electrode and MST coil configurations, the complete 3-D head models incorporating ECT electrodes or MST coil were adaptively tessellated to construct realistic finite element models using the restricted Delaunay triangulation algorithm [28, 34, 47].

The methodologies to simulate the E-field strength induced by ECT and MST are described in detail in our previous studies [17, 28] and are summarized here. Since the current waveform frequencies in ECT and MST are relatively low (<10 kHz), the E-field solutions were obtained by deploying the quasi-static approximation using the finite element analysis software ANSYS (ANSYS Inc., Canonsburg, PA, USA). For ECT, the spatial distribution of the E-field induced by each of the five ECT electrode configurations was computed using the preconditioned conjugate gradient (PCG) solver. We simulated the E-field strength for current amplitude of 800 mA for BL, BF, and RUL ECT (conventional in clinical practice); 612 mA for FEAST (average current amplitude in [14]); and 500 mA for FM ECT (as used in [16]). For MST, a time-harmonic simulation at 5 kHz using the PCG solver was first carried out to compute the spatial E-field distribution generated by CIRC MST, yielding a distribution with unadjusted amplitude. The E-field was then scaled to match the output at maximum amplitude (MA) of the pulses generated by a Magstim Theta device [17].

2.6. Stimulation strength and focality analysis

We analyzed the E-field characteristics in the whole brain (gray and white matter) and in various brain ROIs that have putative role in the mechanisms of action of ECT and MST [28]. The E-field was determined in specific brain ROIs thought to be associated with

therapeutic effects of ECT and MST, including frontal pole, orbitofrontal cortex (OFC), dorsolateral prefrontal cortex (DLPFC), thalamus, hypothalamus, and subcallosal cingulate cortex (SCC) [48–54], or with adverse side effects, including hippocampus and insula [7, 13, 55, 56]. We also sampled the E-field in the first dorsal interosseous (FDI) motor area in motor cortex and in brainstem, which are considered important in seizure initiation and motor manifestations of the seizure, respectively [57, 58]. These ten anatomically defined ROIs were semi-automatically segmented using manual editing tools in ITK-SNAP [36] based on human brain atlases [59], and were verified with BrainParser [60] and the FIRST tool in FSL [61].

We calculated the stimulation strength relative to a neural activation threshold by dividing the E-field magnitude by an E-field threshold, E/E_{th}. We used published estimates of the E-field thresholds for ECT and MST derived in our previous study [17]. In brief, E-field thresholds specific to the pulse widths and shapes of the respective stimulation devices were estimated based on recorded E-field waveforms in combination with neuronal time constant and E-field activation threshold data extracted from TMS studies. This approach effectively creates a “strength–duration” curve that adjusts the E-field threshold for specific pulse shape and width. The estimated E-field thresholds are 0.25 V/cm for ultrabrief pulse ECT (rectangular pulse width = 0.3 ms) and 0.64 V/cm for CIRC MST (cosine pulse duration = 0.4 ms), respectively [17]. For other pulse widths, E_{th} can be scaled with the methods by Deng et al. [17]. For example, for brief pulse (1 ms) ECT, E_{th} = 0.21 V/cm. Therefore, the reported stimulation strength results can be adjusted for brief pulse ECT by multiplying them by 1.17. As an alternative threshold associated with more robust neural activation, we used $1.4\times E_{th}$ [17, 62], which approaches the average threshold values we estimated in a nonhuman primate study [63]. We further compared the ratio of the right-to-left hemispheric E-field stimulation strength among the various ECT electrode and MST coil configurations. Finally, we quantified the focality of stimulation by the percentage of the brain volume exposed to E-field magnitude stronger than the neural activation threshold and the robust neural activation threshold, i.e., the subvolume where $E/E_{th} \geq 1$ and $E/(1.4\times E_{th}) \geq 1$, respectively. To evaluate the effect on the stimulated brain subvolume of altering the pulse amplitude, the E-field simulations for all ECT and MST modalities were scaled linearly to span the range of 0–900 mA and 0–100% MA, respectively, and the subvolume where $E/E_{th} \geq 1$ was computed for these ranges.

3. Results

3.1. Stimulation strength and focality for fixed current amplitude

Figure 2 shows the simulated BL, BF, RUL, FEAST, and FM ECT electrode configurations as well as the CIRC MST coil configuration. The corresponding spatial distributions of the stimulation strength (E-field magnitude relative to the neural activation threshold E_{th}) at nominal current amplitude are shown in representative plots for each modality. Consistent with prior studies in realistic high-resolution head models [28, 64], the E-field distributions vary widely across stimulation configurations and appear to be strongly affected by the anatomy of the head and the conductivity of the various tissues.

Figure 3 shows descriptive statistics of the stimulation strength in various brain ROIs for the ECT and MST modalities. The median stimulation strength relative to threshold is 1.8–2.9 for the conventional ECT paradigms (BL, BF, and RUL at 800 mA), 0.9–1.2 for the experimental ECT paradigms (FM at 500 mA and FEAST at 612 mA), and only 0.3 for CIRC MST [Figure 3(A)]. The maximum stimulation strength of ECT is up to 15 times higher than that for MST. The conventional forms of ECT produce stronger median stimulation than MST in all evaluated ROIs. This is also true for the comparison of MST with the experimental FEAST and FM ECT paradigms, except in the FDI motor area where MST is 10%–70% stronger [Figure 3(J)]. As well, the differences between conventional ECT and MST are smallest in the FDI motor area, with conventional ECT stimulating only 40%–70% stronger than MST. In prefrontal and frontal areas including frontal pole, OFC, and DLFPC [Figures 3(B)–(D)] the median ECT stimulation strength ranges from 2.0 to 5.8 times threshold corresponding to FM and BF ECT, respectively, whereas the values for CIRC MST are much lower, ranging from 0.3 to 0.8 times threshold. In subcortical structures including thalamus and hypothalamus [Figures 3(E)–(F)] the median stimulation strength of ECT ranges from 0.9 to 3.3 times threshold, corresponding to FM and RUL ECT, respectively, while only 0.1–0.3 times threshold for CIRC MST. In SCC [Figure 3(G)] the median stimulation strength of ECT is 9.5–19 times higher than that for MST, with most intense stimulation delivered by BL ECT (2.9 times threshold). BL ECT has the highest median stimulation strength in the hippocampi [Figure 3(H)] and insular cortices [Figure 3(I)], respectively 1.4–20 and 1.4–14 times stronger than the other electrode and coil configurations. FM ECT has the weakest stimulation strength there compared to the other ECT configurations (0.9 times threshold), likely due to the lower-than-standard current amplitude of 500 mA as well as the focal electrode configuration. For CIRC MST, the stimulation strength is even lower—0.2 times threshold in both hippocampi and insular cortices. In brainstem, the median stimulation strength of ECT is 0.7–2.5 times threshold [Figure 3(K)]. This is much higher than the median stimulation of only 9.4% of threshold induced there by CIRC MST, which is the lowest intensity of any ROI for MST.

To quantify the lateralization of stimulation, the ratio of the right to left hemisphere median E-field strength for the various ECT electrode and MST coil configurations is shown in Figure 4. As expected, the ratio for the lateralized electrode configurations (RUL and FEAST) is on average 1.7 times higher compared to the other electrode and coil configurations, demonstrating the stronger stimulation in the right hemisphere, as illustrated in Figure 2.

To quantify the overall focality of stimulation, the percentage of brain volume stimulated above the neural activation threshold ($E \geq E_{th}$) and the robust neural activation threshold ($E \geq 1.4 \times E_{th}$) is shown in Figure 5. Among the ECT paradigms, BL at 800 mA stimulates the largest brain subvolume (99%), while FM at 500 mA produces the most focal brain stimulation (47%). CIRC MST produces more focal stimulation (21%) than all of the ECT modalities. Thus, the stimulation by MST is 3–9 times weaker [Figure 3(A)] and 2–5 times more focal than the ECT paradigms with nominal current amplitude. When applying the E-field threshold for robust neural activation to the E-field distribution ($E \geq 1.4 \times E_{th}$), the percentage of brain volume that is directly stimulated decreases by 3–42% for ECT and by 40% for MST.

3.2. Effect of current amplitude on stimulation strength and focality

Figure 6 shows representative E-field stimulation strength plots for ECT and MST current amplitudes in the range of 200–900 mA and 20–100% MA, respectively. As expected, lowering the current amplitude brings the stimulation closer to the neural activation threshold. Whereas the E-field strength scales linearly with the amplitude of the ECT-electrode or MST-coil current, the relationship between the current amplitude and the percentage of brain volume above the E-field threshold for neural activation ($E \geq E_{th}$) is nonlinear [12], as shown in Figure 7. At the conventional ECT current amplitudes of 800 mA and 900 mA, almost the entire brain is exposed to suprathreshold E-field strength in BL and RUL ECT. Figure 7 demonstrates that lowering the current amplitude reduces the directly stimulated brain subvolume. The slope of the curves in Figure 7 indicates that the ability to control the focality of stimulation is more prominent with ECT configurations with closer electrode spacing (RUL, BF, FM, FEAST) as compared to widely spaced electrodes (BL), which is expected since closer electrode spacing is intrinsically more focal [12].

For the ranges of currents used in the clinical FEAST study (400–800 mA) [14], the median stimulation strength of FEAST in the brain ranges from 0.8 to 1.6 times threshold, corresponding to stimulation of 44% to 89% of the brain, respectively. Of note, this estimate of the focality range is confounded by the fact that in the clinical FEAST study the current was set at the individual amplitude-titrated seizure threshold, which can reduce the E-field variability in the brain resulting from individual differences. Experimentally, RUL ECT has been applied with 500 mA current [20–22]. For this configuration, the median stimulation strength in the brain is 1.2 times neural activation threshold, corresponding to stimulation of 81% of the brain volume. Based on the simulation results for the various ECT electrode configurations, current amplitudes below 217–561 mA, corresponding to BL and FM respectively, were estimated to produce subthreshold median field strength in hippocampus. Finally, ECT current amplitudes of 192–311 mA, corresponding to BL and FM respectively, resulted in approximately matched focality with MST at 100% MA.

4. Discussion

This work contributes a quantitative comparison of the stimulation characteristics of standard and experimental ECT configurations as well as MST using a high resolution, anatomically accurate, finite element human head model combined with estimated, modality-specific neural activation thresholds. These interventions have been shown experimentally to induce generalized seizures, while having different therapeutic efficacy and side effect profiles. The substantial differences in the E-field characteristics across interventions revealed in our simulations highlight the importance of understanding the relationship between stimulation parameters and clinical outcome, as well as optimization of the parameters for robust efficacy and reduced side effects.

4.1. Standard ECT configurations

The standard ECT configurations (BL, RUL, BF) produced the strongest overall stimulation with median strength over 1.8 times threshold and suprathreshold strength in 94% of the brain volume for conventional current amplitude of 800–900 mA and ultrabrief pulse width

(0.3 ms). For brief pulse width (1 ms), the median strength is 17% higher, corresponding to even larger stimulated brain subvolume. Of note, this scaling factor is based on the assumption of dominant axonal stimulation effects, whereas for high E-field strengths more prominent differences in effect on other neural elements (soma and dendrites) between ultrabrief and brief pulses may be relevant as well [18]. In any case, for both ultrabrief and brief pulses the median E-field strength is above the neural activation threshold for all analyzed ROIs.

The widespread suprathreshold stimulation of the brain with BL, BF, and RUL ECT at 800 mA, even more prominent for brief than ultrabrief pulses, is much higher than necessary for seizure induction [20–22, 65] and may contribute to the adverse side effects of ECT. Moreover, it could explain why some studies found few differences in the cognitive side effects of these paradigms [13, 66]. While frontal brain areas are a rational therapeutic target for ECT [54], their stimulation could potentially contribute to cognitive deficits, specifically executive dysfunction, as well. We found that stimulation is strong or stronger in frontal regions (OFC, DLPFC, frontal pole) with BF ECT compared to BL ECT, which could explain the lack of cognitive advantages of the former reported in some studies [4, 13]. RUL ECT generates weaker hippocampal E-field than BL ECT, consistent with fewer memory deficits resulting from RUL ECT [7, 11, 13]. Furthermore, RUL ECT produces 50% weaker stimulation in the left hippocampus than in the right hippocampus, which potentially contributes to cognitive sparing as well.

4.2. MST

In contrast to the standard ECT paradigms (BL, RUL, and BF configurations at 800–900 mA), the median stimulation strength of MST is lower than the neural activation threshold is all analyzed ROIs except for the FDI motor area. Consequently, CIRC MST stimulates only 21% of the brain volume. Thus, MST produces relatively focal stimulation, but is nevertheless capable of inducing generalized seizures and has antidepressant effect. Notably, the stimulation in the hippocampi by MST is 11–20 times weaker than the ECT paradigms, which could explain the fewer memory side effects of MST. Furthermore, the reduced stimulation strength in frontal regions (OFC, DLPFC, frontal pole) with MST relative to ECT could protect executive function.

On the other hand, modulation of frontal areas as well as deeper structures such as thalamus, hypothalamus, SCC, and hippocampus is hypothesized to be associated with the antidepressant effects of ECT [49–54, 67, 68]. In these areas, MST generates stimulation that is 3–29 times weaker than standard ECT (by > 3 times for frontal areas and > 6 times for the deeper areas). The fact that MST had an antidepressant effect with suprathreshold stimulation of a limited extent of superficial cortex suggests that direct suprathreshold stimulation of deeper targets may not be necessary or indirect transsynaptic stimulation may suffice for therapeutic effect.

4.3. ECT technique modifications

Experimental interventions such as MST, FEAST [14], and low-amplitude ECT [16, 20–22, 65] are predicated on reducing the electricity exposure in the brain by making the E-field

weaker and more focal to diminish the side effects of ECT. Consistent with the demonstrated ability of these interventions to induce seizures, our results show that their E-field is suprathreshold in a significant portion of the brain. Enabling further exploration of dosing approaches, we quantified how lowering the stimulus current amplitude reduces the stimulation strength in the brain and increases the focality of stimulation. By lowering the current amplitude in ECT, its focality can match that of MST. The control over focality using the current amplitude is most effective with intrinsically more focal ECT electrode placements like RUL, BF, FM, and FEAST as opposed to BL. For example, the combination of focal ECT electrode placements and reducing the stimulus current amplitude 2–4 fold could be used to avoid direct stimulation of the hippocampi, which could spare memory circuits, while still strong enough to induce a seizure.

These observations support the potential of low-current-amplitude ECT as an alternative means to reduce side effects. They are consistent with the results from our spherical head models where we demonstrated that ECT with adjusted electrode size and spacing and current of 300 mA can match the stimulation strength, focality, and depth of MST with a double cone coil [12]. ECT has technological advantages over MST since, compared to transcranial magnetic stimulation, transcranial electric stimulation expends 10^{-4} times less energy to deliver the same amount of energy to the brain [69]. Consequently, an ECT device is simpler, cheaper, and unconstrained by coil heating and insulation issues. Maximum focality, however, will require an extended range of low current amplitudes below the 500 mA limit available in commercial ECT devices, as well as potentially reduced electrode size and spacing [12, 14].

The reduced stimulation intensity at lower currents may decrease the side effects of convulsive therapies, but may also impact therapeutic efficacy [4]. Even the same E-field strength and distribution can have widely varying efficacy and side effects depending on other stimulus parameters such as the number of pulses relative to the seizure threshold [11]. There may be complex contributions and interactions of the spatial and temporal aspects of ECT and MST dose and the resultant seizures that affect the efficacy and side effects of novel stimulus configurations. Therefore the outcomes of low-current-amplitude ECT paradigms have to be examined ultimately in clinical trials, with proper consideration given to the other current parameters as well.

Finally, our simulations are directly applicable to the revived interest in treatment with intense but subconvulsive stimulation trains [70, 71], where the characteristics of the E-field may be even more important than in conventional ECT as no generalized seizure is induced and, hence, the effects are limited to those of the E-field. Regenold et al. delivered subconvulsive stimulation with standard BF ECT electrode placement and 900 mA, 0.5 ms pulses [70]. This paradigm appears to stimulate most of the brain volume, as indicated in Figures 6 and 7, especially considering that the pulse width was longer than in the simulations (0.3 ms). Thus, it could be speculated that this intervention has spatially extended, synchronous stimulatory effects that parallel those of a generalized seizure, but over a much shorter duration equal to the length of the electrical stimulus.

4.4. Limitations

This type of modeling has general limitations that were discussed in our prior studies [12, 17, 28, 63]. The effects of ECT and MST are understood to result from two principal processes: (1) the activation of neurons with E-field pulse trains and (2) the resultant seizure initiation and propagation. Of these, our models capture only the approximate strength of neuron activation by each pulse within the stimulus train. The models do not account for either the cumulative effect of the multiple pulses or for the subsequent seizure initiation and generalization. Nevertheless, if the E-field is subthreshold in a particular region, it is unlikely that a seizure initiation or other strong neuromodulatory effects can occur there. On the other hand, the presence of a suprathreshold E-field does not directly indicate that a seizure would be initiated in this region or what the seizure initiation threshold in terms of number of pulses is. Modeling these processes for the whole brain is not feasible at present.

The present study does not account for anatomical variability of the ECT and MST clinical populations. Since we used a head model of a single individual, we did not explore to what extent the current amplitude should be individualized to compensate for individual anatomical variability. Our prior computational modeling and preclinical studies suggest that current amplitude individualization is indeed appropriate in order to normalize the E-field exposure across individuals [12, 63, 65, 72, 73]. The methodologies presented in this paper are general and can be applied to any number of individuals in future studies.

Only one MST coil configuration [38] was modeled, whereas other clinical MST sudies have used different coil configurations [27]. In our prior spherical head model studies we did simulate several additional MST coil configurations [12, 17, 72], which, combined with the results for this study can provide an estimate of how the stimulation characteristics change. Generally, our prior modeling suggests that the superficiality and weaker stimulation strength is shared among various MST coil configurations as compared to conventional ECT, although the double-cone and cap coils induce stronger and less focal stimulation than the double-layer circular coil [17, 72]. Finally, other MST coil configurations and stimulation devices can be simulated using the described methods.

5. Conclusions

This paper quantified the effect of electrode/coil configuration and current amplitude on the stimulation induced in the brain by both conventional and experimental ECT paradigms as well as by MST. It confirms and extends previous findings that (1) conventional ECT stimulates directly a large proportion of the brain volume at strengths exceeding markedly the neural activation threshold; (2) RUL electrode placement produces weaker overall stimulation of the hippocampi compared to BL ECT, potentially explaining cognitive sparing with RUL ECT; (3) MST induces more focal and weaker stimulation compared to both conventional as well as several experimental ECT paradigms, which could contribute to the reduction of cognitive side effects in MST compared to ECT; and (4) lowering the ECT current amplitude enables stimulation that is more focal and closer to the neural activation threshold, and can approximate MST. This work could help understand the mechanisms of conventional ECT as well as the development of alternative approaches with superior risk/benefit ratio.

Acknowledgments

This work was supported by the National Institutes of Health under grant R01MH091083 and an ANSYS Strategic Research Partnership. The authors thank Drs. Paolo Maccarini and Murali Kadiramangalam for the ANSYS license donation.

References

1. Weiner, RD. Introduction to Convulsive Therapy. In: Reti, IM., editor. Brain Stimulation: Methodologies and Interventions. Wiley Blackwell; 2015. p. 61-82.
2. Ingram A, Saling MM, Schweitzer I. Cognitive side effects of brief pulse electroconvulsive therapy: a review. J ECT. 2008; 24:3–9. [PubMed: 18379328]
3. Semkovska M, McLoughlin DM. Objective cognitive performance associated with electroconvulsive therapy for depression: a systematic review and meta-analysis. Biol Psychiatry. 2010; 68:568–77. [PubMed: 20673880]
4. Rasmussen, KG. Improving ECT Efficacy and Decreasing Cognitive Side Effects. In: Reti, IM., editor. Brain Stimulation: Methodologies and Interventions. Wiley Blackwell; 2015. p. 83-106.
5. Liberson WT. Brief stimulus therapy; psysiological and clinical observations. Am J Psychiatry. 1948; 105:28–39. [PubMed: 18874254]
6. Weiner RD, Rogers HJ, Davidson JR, Squire LR. Effects of stimulus parameters on cognitive side effects. Ann N Y Acad Sci. 1986; 462:315–25. [PubMed: 3458412]
7. Sackeim HA, Prudic J, Nobler MS, Fitzsimons L, Lisanby SH, Payne N, et al. Effects of pulse width and electrode placement on the efficacy and cognitive effects of electroconvulsive therapy. Brain Stimul. 2008; 1:71–83. [PubMed: 19756236]
8. Cronholm B, Ottosson JO. Ultrabrief stimulus technique in electroconvulsive therapy. I. Influence on retrograde amnesia of treatments with the Elther ES electroschock apparatus, Siemens Konvulsator III and of lidocaine-modified treatment. J Nerv Ment Dis. 1963; 137:117–23. [PubMed: 14047818]
9. Cronholm B, Ottosson JO. Ultrabrief stimulus technique in electroconvulsive therapy. II. Comparative studies of therapeutic effects and memory disturbances in treatment of endogenous depression with the Elther ES electroshock apparatus and Siemens Konvulsator III. J Nerv Ment Dis. 1963; 137:268–76. [PubMed: 14051942]
10. Loo CK, Sainsbury K, Sheehan P, Lyndon B. A comparison of RUL ultrabrief pulse (0.3 ms) ECT and standard RUL ECT. Int J Neuropsychopharmacol. 2008; 11:883–90. [PubMed: 18752719]
11. Sackeim HA, Prudic J, Devanand DP, Nobler MS, Lisanby SH, Peyser S, et al. A prospective, randomized, double-blind comparison of bilateral and right unilateral electroconvulsive therapy at different stimulus intensities. Arch Gen Psychiat. 2000; 57:425–34. [PubMed: 10807482]
12. Deng ZD, Lisanby SH, Peterchev AV. Controlling stimulation strength and focality in electroconvulsive therapy via current amplitude and electrode size and spacing: comparison with magnetic seizure therapy. J ECT. 2013; 29:325–35. [PubMed: 24263276]
13. Kellner CH, Knapp R, Husain MM, Rasmussen K, Sampson SCM, McClintock SM, et al. Bifrontal, bitemporal and right unilateral electrode placement in ECT: randomised trial. Br J Psychiatry. 2010; 196:226–34. [PubMed: 20194546]
14. Nahas Z, Short B, Burns C, Archer M, Schmidt M, Prudic J, et al. A feasibility study of a new method for electrically producing seizures in man: focal electrically administered seizure therapy [FEAST]. Brain Stimul. 2013; 6:403–8. [PubMed: 23518262]
15. Spellman T, Peterchev AV, Lisanby SH. Focal electrically administered seizure therapy: a novel form of ECT illustrates the roles of current directionality, polarity, and electrode configuration in seizure induction. Neuropsychopharmacology. 2009; 34:2002–10. [PubMed: 19225453]
16. Rosa MA, Abdo GL, Rosa MO, Lisanby SH, Peterchev AV. Fronto-medial electrode placement with low current amplitude: a case report. J ECT. 2012; 28:146.
17. Deng ZD, Lisanby SH, Peterchev AV. Electric field strength and focality in electroconvulsive therapy and magnetic seizure therapy: a finite element simulation study. J Neural Eng. 2011; 8:016007. [PubMed: 21248385]

18. Peterchev AV, Rosa MA, Deng ZD, Prudic J, Lisanby SH. Electroconvulsive therapy stimulus parameters: rethinking dosage. J ECT. 2010; 26:159–74. [PubMed: 20805726]
19. Liberson WT. Current evaluation of electric convulsive therapy; correlation of the parameters of electric current with physiologic and psychologic changes. Res Publ Assoc Res Nerv Ment Dis. 1953; 31:199–231. [PubMed: 13038103]
20. Rosa MA, Abdo GL, Lisanby SH, Peterchev AV. Seizure induction with low-amplitude-current (0. 5A) electroconvulsive therapy. J ECT. 2011; 27:341–2.
21. Youssef NA, Sidhom E. Examination of Cognitive Profile and Variability in the Current Amplitude Domain of Low Current Amplitude ECT. Biol Psychiat. 2014; 75:259s–60s.
22. Mayur P, Harris A, Gangadhar B. 500-mA ECT-A Proof of Concept Report. J ECT. 2015; 31:e23–6.
23. Lisanby SH, Luber B, Schlaepfer TE, Sackeim HA. Safety and feasibility of magnetic seizure therapy (MST) in major depression: randomized within-subject comparison with electroconvulsive therapy. Neuropsychopharmacology. 2003; 28:1852–65. [PubMed: 12865903]
24. Fitzgerald PB, Hoy KE, Herring SE, Clinton AM, Downey G, Daskalakis ZJ. Pilot study of the clinical and cognitive effects of high-frequency magnetic seizure therapy in major depressive disorder. Depress Anxiety. 2013; 30:129–36. [PubMed: 23080404]
25. Kayser S, Bewernick BH, Matusch A, Hurlemann R, Soehle M, Schlaepfer TE. Magnetic seizure therapy in treatment-resistant depression: clinical, neuropsychological and metabolic effects. Psychol Med. 2015; 45:1073–92. [PubMed: 25420474]
26. Kayser SB, BH, Grubert C, Hadrysiewicz BL, Axmacher N, Schlaepfer TE. Antidepressant effects, of magnetic seizure therapy and electroconvulsive therapy, in treatment-resistant depression. J Psychiatr Res. 2011; 45:569–76. [PubMed: 20951997]
27. Cretaz E, Brunoni AR, Lafer B. Magnetic Seizure Therapy for Unipolar and Bipolar Depression: A Systematic Review. Neural Plast. 2015; 2015:521398. [PubMed: 26075100]
28. Lee WH, Deng ZD, Kim TS, Laine AF, Lisanby SH, Peterchev AV. Regional electric field induced by electroconvulsive therapy in a realistic finite element head model: influence of white matter anisotropic conductivity. Neuroimage. 2012; 59:2110–23. [PubMed: 22032945]
29. Loo CK, Bai S, Donel MM, Galvez V, Dokos S. Revisiting Frontoparietal Montage in Electroconvulsive Therapy: Clinical Observations and Computer Modeling: A Future Treatment Option for Unilateral Electroconvulsive Therapy. J ECT. 2014
30. Bai S, Loo C, Dokos S. A computational model of direct brain stimulation by electroconvulsive therapy. Conf Proc IEEE Eng Med Biol Soc. 2010; 2010:2069–72. [PubMed: 21095945]
31. Lee WH, Lisanby SH, Laine AF, Peterchev AV. Stimulation Strength and Focality of Electroconvulsive Therapy and Magnetic Seizure Therapy in a Realistic Head Model. Conf Proc IEEE Eng Med Biol Soc. 2014; 2014:410–3. [PubMed: 25569983]
32. Tustison NJ, Avants BB, Cook PA, Zheng Y, Egan A, Yushkevich PA, et al. N4ITK: improved N3 bias correction. IEEE Trans Med Imaging. 2010; 29:1310–20. [PubMed: 20378467]
33. Lee WH, Kim TS, Cho MH, Ahn YB, Lee SY. Methods and evaluations of MRI content-adaptive finite element mesh generation for bioelectromagnetic problems. Phys Med Biol. 2006; 51:6173–86. [PubMed: 17110778]
34. Lee WH, Kim TS. Methods for high-resolution anisotropic finite element modeling of the human head: automatic MR white matter anisotropy-adaptive mesh generation. Med Eng Phys. 2012; 34:85–98. [PubMed: 21820347]
35. Smith SM. Fast robust automated brain extraction. Hum Brain Mapp. 2002; 17:143–55. [PubMed: 12391568]
36. Yushkevich PA, Piven J, Hazlett HC, Smith RG, Ho S, Gee JC, et al. User-guided 3D active contour segmentation of anatomical structures: significantly improved efficiency and reliability. Neuroimage. 2006; 31:1116–28. [PubMed: 16545965]
37. Zhang YY, Brady M, Smith S. Segmentation of brain MR images through a hidden Markov random field model and the expectation-maximization algorithm. Ieee T Med Imaging. 2001; 20:45–57.

38. Kirov G, Ebmeier KP, Scott AI, Atkins M, Khalid N, Carrick L, et al. Quick recovery of orientation after magnetic seizure therapy for major depressive disorder. Br J Psychiatry. 2008; 193:152–5. [PubMed: 18670002]
39. Gabriel C, Gabriel S, Corthout E. The dielectric properties of biological tissues: I. Literature survey. Phys Med Biol. 1996; 41:2231–49. [PubMed: 8938024]
40. Wolters CH, Anwander A, Tricoche X, Weinstein D, Koch MA, MacLeod RS. Influence of tissue conductivity anisotropy on EEG/MEG field and return current computation in a realistic head model: A simulation and visualization study using high-resolution finite element modeling. Neuroimage. 2006; 30:813–26. [PubMed: 16364662]
41. Awada KA, Jackson DR, Baumann SB, Williams JT, Wilton DR, Fink PW, et al. Effect of conductivity uncertainties and modeling errors on EEG source localization using a 2-D model. Ieee T Bio-Med Eng. 1998; 45:1135–45.
42. Sadleir RJ, Vannorsdall TD, Schretlen DJ, Gordon B. Transcranial direct current stimulation (tDCS) in a realistic head model. Neuroimage. 2010; 51:1310–8. [PubMed: 20350607]
43. Hallez H, Staelens S, Lemahieu I. Dipole estimation errors due to not incorporating anisotropic conductivities in realistic head models for EEG source analysis. Phys Med Biol. 2009; 54:6079–93. [PubMed: 19779215]
44. Hallez H, Vanrumste B, Van Hese P, Delputte S, Lemahieu I. Dipole estimation errors due to differences in modeling anisotropic conductivities in realistic head models for EEG source analysis. Phys Med Biol. 2008; 53:1877–94. [PubMed: 18364544]
45. Tuch DS, Wedeen VJ, Dale AM, George JS, Belliveau JW. Conductivity mapping of biological tissue using diffusion MRI. Ann N Y Acad Sci. 1999; 888:314–6. [PubMed: 10842642]
46. Tuch DS, Wedeen VJ, Dale AM, George JS, Belliveau JW. Conductivity tensor mapping of the human brain using diffusion tensor MRI. Proc Natl Acad Sci U S A. 2001; 98:11697–701. [PubMed: 11573005]
47. Pons JP, Segonne E, Boissonnat JD, Rineau L, Yvinec M, Keriven R. High-quality consistent meshing of multi-label datasets. Inf Process Med Imaging. 2007; 20:198–210. [PubMed: 17633700]
48. Abrams, R. Electroconvulsive therapy. 4. New York: Oxford Unversity Press; 2002.
49. Abrams R, Taylor MA. Diencephalic stimulation and the effects of ECT in endogenous depression. Br J Psychiatry. 1976; 129:482–5. [PubMed: 791433]
50. Krystal AD, Weiner RD. ECT seizure therapeutic adequacy. Convuls Ther. 1994; 10:153–64. [PubMed: 8069641]
51. Krystal AD, Weiner RD, McCall WV, Shelp FE, Arias R, Smith P. The effects of ECT stimulus dose and electrode placement on the ictal electroencephalogram: an intraindividual crossover study. Biol Psychiatry. 1993; 34:759–67. [PubMed: 8292679]
52. Mayberg HS. Targeted electrode-based modulation of neural circuits for depression. J Clin Invest. 2009; 119:717–25. [PubMed: 19339763]
53. Mayberg HS, Lozano AM, Voon V, McNeely HE, Seminowicz D, Hamani C, et al. Deep brain stimulation for treatment-resistant depression. Neuron. 2005; 45:651–60. [PubMed: 15748841]
54. Sackeim HA. Convulsant and anticonvulsant properties of electroconvulsive therapy: towards a focal form of brain stimulation. Clin Neurosci Res. 2004; 4:39–57.
55. Lisanby SH, Maddox JH, Prudic J, Devanand DP, Sackeim HA. The effects of electroconvulsive therapy on memory of autobiographical and public events. Arch Gen Psychiatry. 2000; 57:581–90. [PubMed: 10839336]
56. Squire LR, Slater PC, Miller PL. Retrograde-amnesia and bilateral electroconvulsive-therapy - long-term follow-up. Arch Gen Psychiat. 1981; 38:89–95. [PubMed: 7458573]
57. Blumenfeld H, Westerveld M, Ostroff RB, Vanderhill SD, Freeman J, Necochea A, et al. Selective frontal, parietal, and temporal networks in generalized seizures. Neuroimage. 2003; 19:1556–66. [PubMed: 12948711]
58. Sackeim HA, Mukherjee S. Neurophysiological variability in the effects of the ECT stimulus. Convuls Ther. 1986; 2:267–76. [PubMed: 11940876]
59. Talairach, J., Tournoux, P. Co-planar stereotaxic atlas of the human brain: 3-dimensional proportional system: an approach to cerebral imaging. Stuttgart; New York: Georg Thieme; 1988.

60. Tu Z, Narr KL, Dollar P, Dinov I, Thompson PM, Toga AW. Brain anatomical structure segmentation by hybrid discriminative/generative models. IEEE Trans Med Imaging. 2008; 27:495–508. [PubMed: 18390346]

61. Patenaude B, Smith SM, Kennedy DN, Jenkinson M. A Bayesian model of shape and appearance for subcortical brain segmentation. Neuroimage. 2011; 56:907–22. [PubMed: 21352927]

62. Pitcher JB, Ogston KM, Miles TS. Age and sex differences in human motor cortex input-output characteristics. J Physiol. 2003; 546:605–13. [PubMed: 12527746]

63. Lee WH, Lisanby SH, Laine AF, Peterchev AV. Electric Field Model of Transcranial Electric Stimulation in Nonhuman Primates: Correspondence to Individual Motor Threshold. IEEE Trans Biomed Eng. 2015

64. Thielscher A, Opitz A, Windhoff M. Impact of the gyral geometry on the electric field induced by transcranial magnetic stimulation. Neuroimage. 2011; 54:234–43. [PubMed: 20682353]

65. Peterchev AV, Krystal AD, Rosa MA, Lisanby SH. Individualized Low-Amplitude Seizure Therapy: Minimizing Current for Electroconvulsive Therapy and Magnetic Seizure Therapy. Neuropsychopharmacology. 2015; 40:2076–84. [PubMed: 25920013]

66. Sienaert P, Vansteelandt K, Demyttenaere K, Peuskens J. Randomized comparison of ultra-brief bifrontal and unilateral electroconvulsive therapy for major depression: cognitive side-effects. J Affect Disord. 2010; 122:60–7. [PubMed: 19577808]

67. McNally KA, Blumenfeld H. Focal network involvement in generalized seizures: new insights from electroconvulsive therapy. Epilepsy Behav. 2004; 5:3–12. [PubMed: 14751200]

68. Reti, IM. How does electroconvulsive therapy work?. In: Reti, IM., editor. Brain Stimulation: Methodologies and Interventions. Wiley Blackwell; 2015. p. 107-22.

69. Jalinous R. Technical and practical aspects of magnetic nerve stimulation. J Clin Neurophysiol. 1991; 8:10–25. [PubMed: 2019644]

70. Regenold WT, Noorani RJ, Piez D, Patel P. Nonconvulsive Electrotherapy for Treatment Resistant Unipolar and Bipolar Major Depressive Disorder: A Proof-of-concept Trial. Brain Stimul. 2015; 8:855–61. [PubMed: 26187603]

71. Sackeim HA. Is the Seizure an Unnecessary Component of Electroconvulsive Therapy? A Startling Possibility. Brain Stimul. 2015; 8:851–4. [PubMed: 26358486]

72. Deng ZD, Lisanby SH, Peterchev AV. Effect of anatomical variability on electric field characteristics of electroconvulsive therapy and magnetic seizure therapy: a parametric modeling study. IEEE Trans Neural Syst Rehabil Eng. 2015; 23:22–31. [PubMed: 25055384]

73. Lee WH, Lisanby SH, Laine AF, Peterchev AV. Electric field characteristics of electroconvulsive therapy with individualized current amplitude: a preclinical study. Conf Proc IEEE Eng Med Biol Soc. 2013; 2013:3082–5. [PubMed: 24110379]

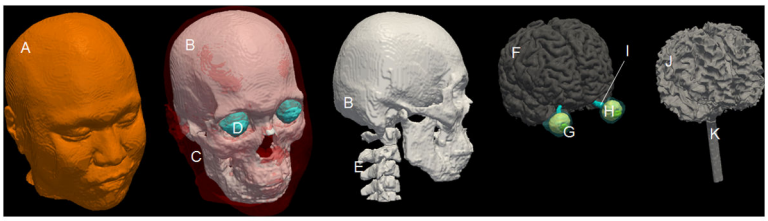

Figure 1.

An individual model of the whole head including various tissue conductivity compartments representing (A) skin, (B) skull compacta, (C) muscle, (D) sclera, (E) vertebrae, (F) gray matter, (G) lens, (H) eyeball, (I) optic nerve, (J) white matter, and (K) spinal cord.

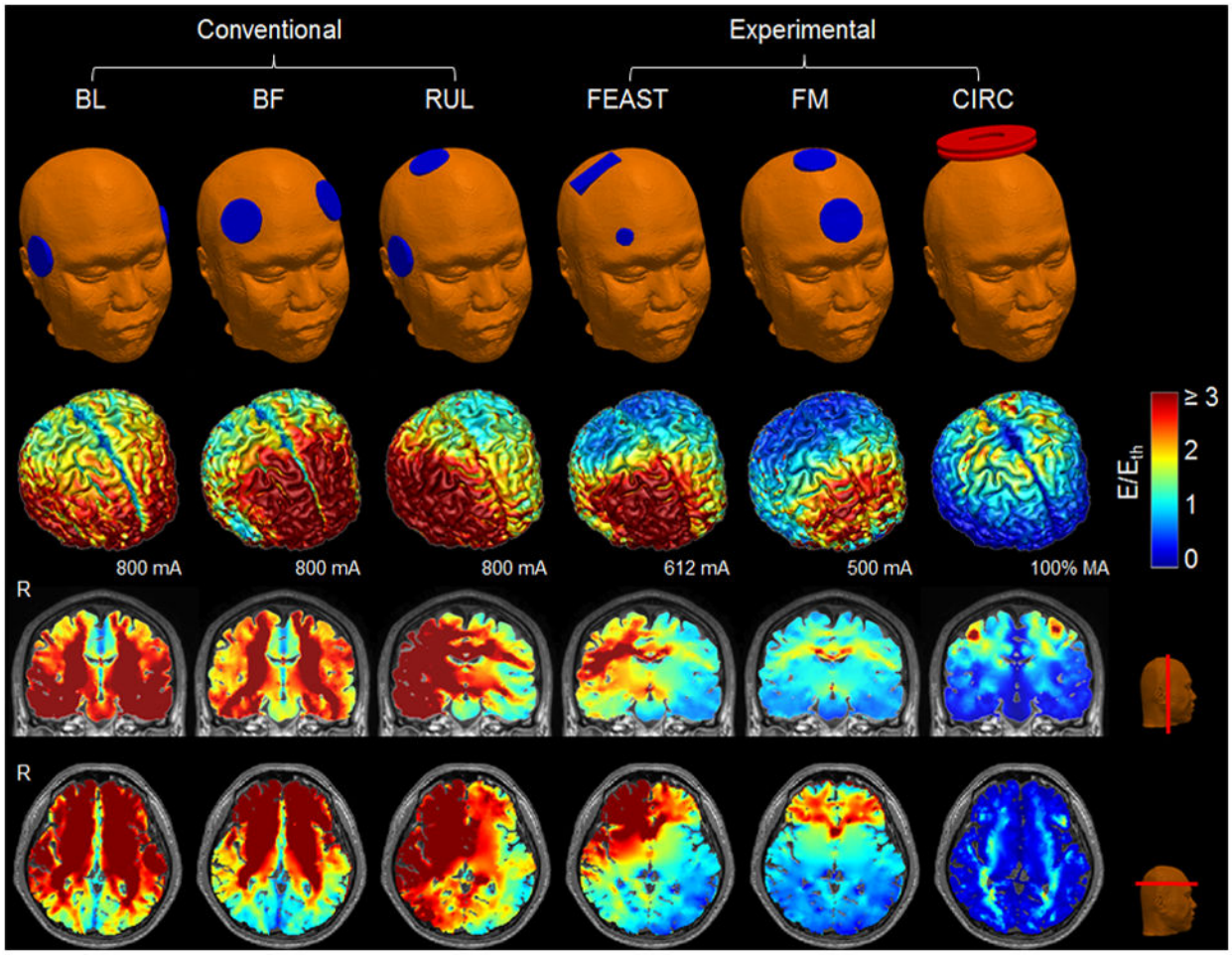

Figure 2.

Simulation models of BL, BF, RUL, FEAST, and FM ECT as well as CIRC MST (top row). Stimulation strength (E-field magnitude relative to neural activation threshold, E/E_{th}) on the cortical surface at current of 800 mA for BL, BF, and RUL ECT, 612 mA for FEAST, 500 mA for FM ECT, and 100% of maximum amplitude (MA) for Magstim Theta with CIRC MST coil configuration (second row), as well as in representative coronal and axial slices (third and bottom rows, respectively). The threshold E_{th} is 0.25 V/cm for ECT (ultrabrief 0.3 ms pulse width) and 0.64 V/cm for MST. For ECT with brief pulse width (1 ms), stimulation strength should be multiplied by 1.17 [17]. The color map is clamped at an upper limit of 3 for good visibility of the spatial distribution. R: right.

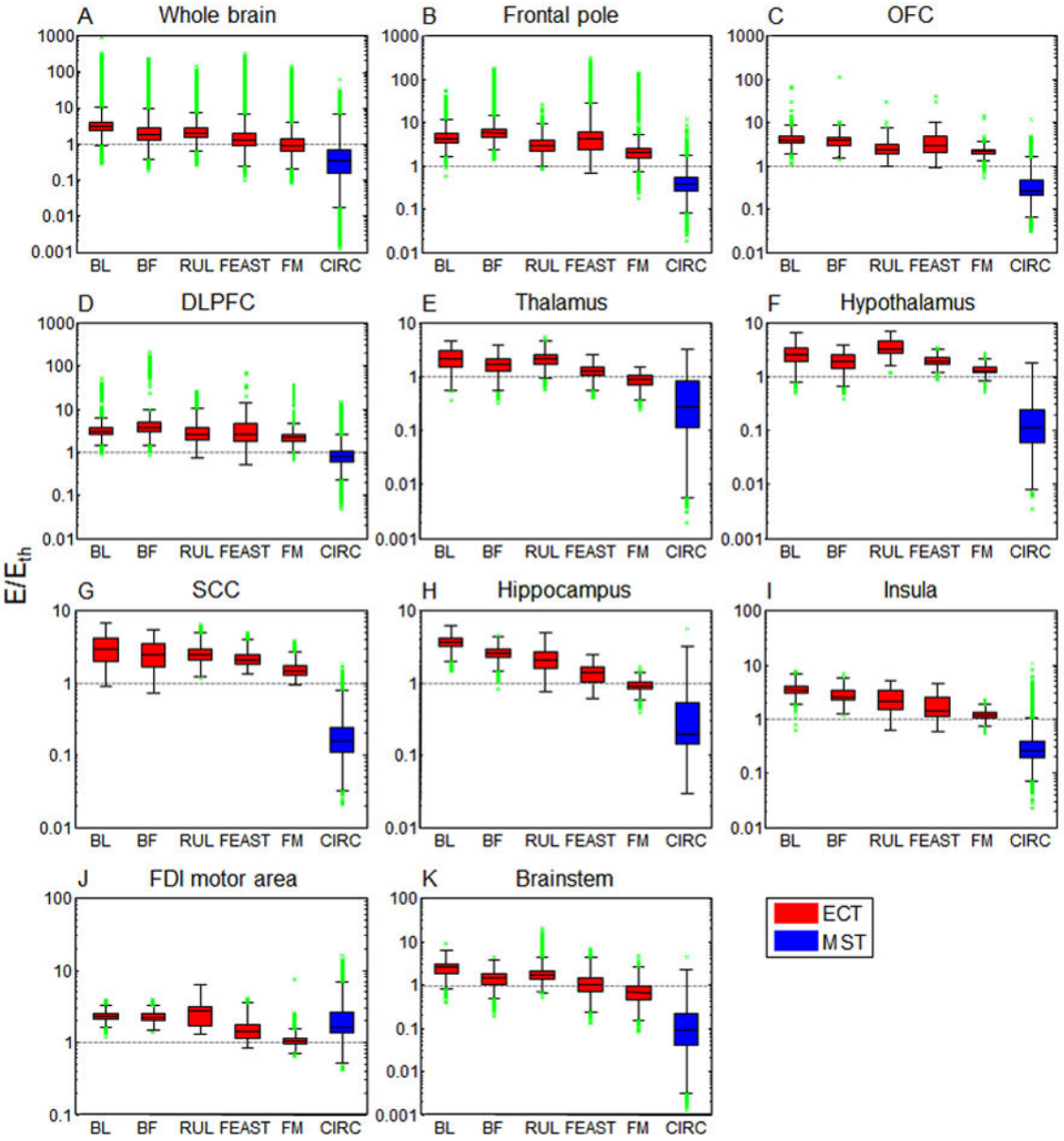

Figure 3.

Descriptive statistics of stimulation strength (E/E_{th}) in specific brain ROIs for the configurations depicted in Figure 2. Boxes indicate the interquartile range (25^{th} to 75^{th} percentile) with the median marked by a horizontal black line. Whiskers delimit approximately the 99.3 percentile of the E-field distribution. Outliers beyond this range are plotted in green. Horizontal gray dotted lines demarcate the boundary between subthreshold and suprathreshold stimulation strength. The ECT results are for ultrabrief pulse width (0.3 ms); for brief pulse width (1 ms), the stimulation strength should be multiplied by 1.17 [17]. OFC: orbitofrontal cortex, DLPFC: dorsolateral prefrontal cortex, SCC: subcallosal cingulate cortex, FDI: first dorsal interosseous.

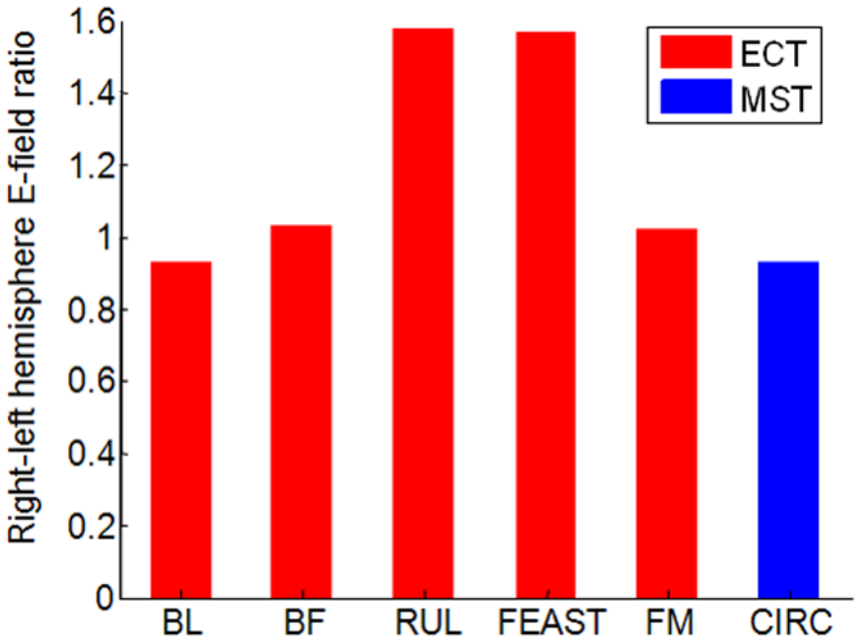

Figure 4.
Ratio of median E-field strength in right relative to left hemisphere for the configurations depicted in Figure 2.

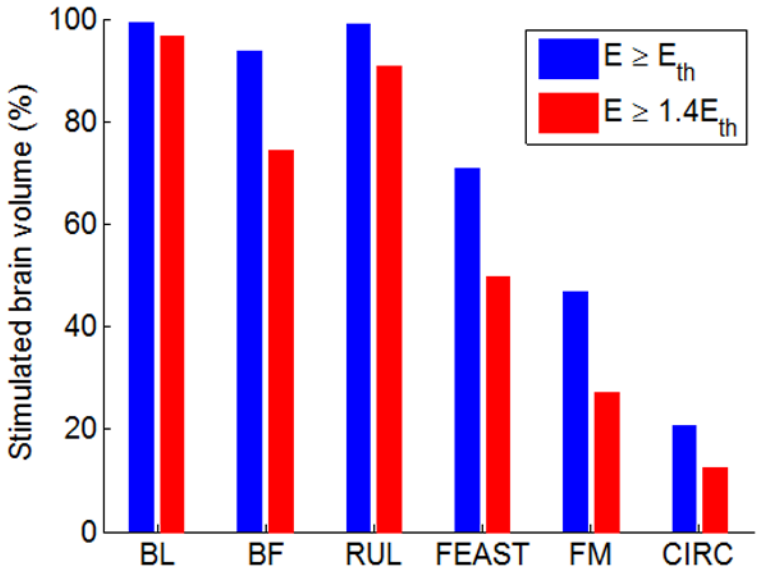

Figure 5.

Percentage of the brain volume stimulated above neural activation threshold ($E \geq E_{th}$) and above robust neural activation threshold ($E \geq 1.4 \times E_{th}$) for the configurations depicted in Figure 2.

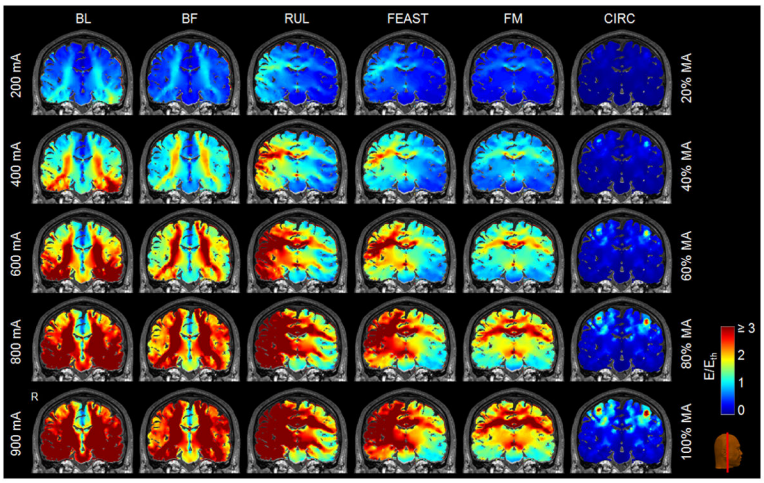

Figure 6.

Stimulation strength (E/E_{th}) of the ECT electrode configurations (first to fifth columns, respectively) and MST coil configuration (sixth column) depicted in Figure 2 for current amplitudes ranging from 200 mA to 900 mA for ECT (ultrabrief 0.3 ms pulse width) and 20% to 100% MA for MST (Magstim Theta device). Color scale is identical to Figure 2.

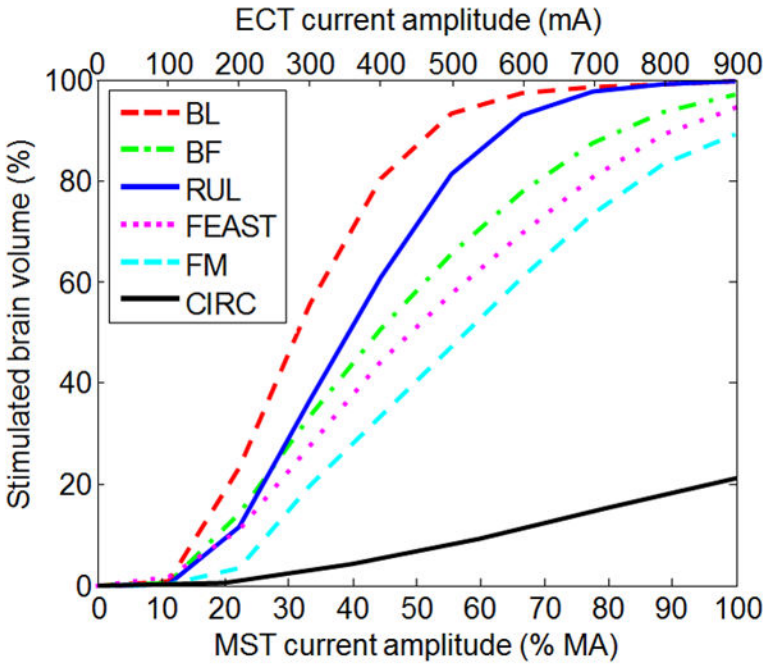

Figure 7.

Percentage of the brain volume stimulated above neural activation threshold ($E \geq E_{th}$) as a function of current amplitude for the configurations depicted in Figures 2 and 6. The ECT results (BL, BF, RUL, FEAST, FM) are for ultrabrief pulse width (0.3 ms). The MST results (CIRC) are for the Magstim Theta device.

Table 1

Tissue electrical conductivities (S/m) used in the model

Tissue	Conductivity	Tissue	Conductivity
Skin	0.43	Lens	0.32
Muscle	0.32	Eyeball	0.5
Skull compacta	0.0063	Sclera	0.5
Skull spongiosa	0.04	Spinal cord	0.15
Cerebrospinal fluid (CSF)	1.79	Vertebrae	0.012
Gray matter	0.33	Optic nerve	0.14
White matter (iso.)	0.14	Sinus	0